Nano Energy 78 (2020) 105279

Contents lists available at ScienceDirect

Nano Energy

journal homepage: http://www.elsevier.com/locate/nanoen

A novel humidity resisting and wind direction adapting flag-type triboelectric nanogenerator for wind energy harvesting and speed sensing

Yan Wang [a,b], En Yang [a], Tianyu Chen [a], Jianye Wang [a], Zhiyuan Hu [a], Jianchun Mi [a,c], Xinxiang Pan [a,b], Minyi Xu [a,*]

[a] Marine Engineering College, Dalian Maritime University, Dalian, 116026, China
[b] School of Electronics and Information Technology, Guangdong Ocean University, Zhanjiang, 524088, China
[c] College of Engineering, Peking University, Beijing, 100871, China

ARTICLE INFO

Keywords:
Triboelectric nanogenerator
Flutter
Wind energy harvesting
Wind speed sensing

ABSTRACTS

Wind energy harvesting from ambient environment by TENG is highly desirable for powering the wireless sensing system. However, humid environment and variable wind direction deteriorate the output performance of the most demonstrated TENG-based wind energy harvesters. In this work, a humidity resisting and wind direction adapting flag-type TENG is to be proposed and investigated. The flag-type TENG consists of two carbon-coated polyethylene terephthalate membranes and one strip of poly tetra fluoroethylene membrane with their edges sealed up. Thus, the triboelectric layers are isolated from the air and the electrical performance is independent of the relative humidity. Parametric studies are conducted to evaluate the influence of geometrical parameters of the flag-type TENG on the flutter behavior and the resulting energy output. It is interesting to find that a pair of flag type TENGs with a certain gap distance can contact with each other due to the wind speed variation and pressure difference between the internal and external flow areas. The power density is increased by 40 times compared with the only one flag-type TENG. In addition, the flag-type TENG can harvest wind energy from arbitrary directions without equipping other extra mechanisms. It can also serve as a self-powered wind speed and direction sensor. Therefore, the present flag-type TENG has a great potential to apply for ambient wind energy harvesting, self-powered wind speed and direction sensing in harsh natural conditions.

1. Introduction

Energy harvesting from ambient environment is a key question for building up the self-powered systems of wireless electronics, mobile electronics and wearable electronics. Traditionally, batteries have been used as the power source for such devices [1,2]. However, billions of batteries produced each year consume countless resources, the disposal of batteries causes severe environmental pollution, and the use of batteries challenges the long-term operation of the devices. Wind energy is a promising source for self-powered devices due to its wide existence in nature and is virtually pollution-free. The conventional wind turbine can effectively harvest wind energy, but mainly for the large-scale grid power supply [3]. A flow-induced vibration energy harvester is a micro-energy harvesting device designed to harness vibration induced by a flow. In general, flow-induced vibration can be divided into four types with different characteristics: i.e., flutter, galloping, vortex-induced vibration and buffeting [4]. In recent years, numerous wind-driven flutter energy harvesters are reported for capturing energy from the surrounding flow field to power a sensing node or a wireless sensing system for continuous monitoring [5–15]. There are many types of wind energy harvesters based on the principle of flutter, such as piezoelectric, electromagnetic and triboelectric. However, due to their high bending stiffness [16] and low cycle life [17] piezoelectric wind energy harvesters are not suitable for those applications where low wind speed and long-term operations are needed. Moreover, large size [18] and complex structure [19] make electromagnetic wind-driven flutter energy harvester unsuitable for application where small space and maintenance-free are needed.

Since its invention in 2012, the triboelectric nanogenerator (TENG) has exhibited great potential as a wind energy harvester due to its low cost [20,21], simple fabrication process [22–24], and good scalability [25,26]. Recently, a number of wind energy TENG harvesters based on flutter membrane have been proposed [27–36]. A flutter-driven triboelectric generator (FTEG) was reported by Bae et al. [37]. They

* Corresponding author.
E-mail address: xuminyi@dlmu.edu.cn (M. Xu).

https://doi.org/10.1016/j.nanoen.2020.105279
Received 2 July 2020; Received in revised form 29 July 2020; Accepted 9 August 2020
Available online 19 August 2020

experimentally investigated the effect of wind speed on output performance. The FTEG was promising to harvest wind energy for its simple fabrication process, very low cost and less weight [37]. Wang et al. [38] proposed an elasto-aerodynamics-driven TENG to scavenge air-flow energy. The energy can be harvested from human breath by the fabricated TENG to drive a thermometer. Perez et al. [39] proposed a flutter-and-electret-based energy harvester. They investigated the influence of mass ratio and aspect ratio on self-sustained fluttering. Their device could reach the output power of 178 $\mu W/cm^3$ at 15 m/s and 782 $\mu W/cm^3$ at 30 m/s. The maximum power coefficient is 0.54% at 15 m/s, which is comparable to other small-scale wind energy harvesters. However, the flutter membrane and electrode of above TENGs are fixed in a frame structure, and thus limit the capacity to harvest wind energy from arbitrary directions. Zhao et al. [40] introduced a freestanding woven triboelectric nanogenerator flag (WTENG flag) with Ni-belt electrode to harvest wind energy from arbitrary direction. The fluttering of the WTENG flag leads to relative contact-separation motion between the Kapton film and Ni-belt. Due to its rigidity, it's adaptable only in high-altitude and high-wind-speed. Meanwhile, the output performance of the WTENG flag decrease sharply when the humidity increases. Similarly, most of demonstrated TENGs are sensitive to humidity [29,41–44]. Therefore, a new type of wind energy TENG is in high demand that can effectively harvest wind energy from arbitrary directions in high humidity condition.

To address this need, the present work is conducted to propose and systematically investigate a humidity resisting and wind direction adapting flag-type TENG consisting of two carbon-coated polyethylene terephthalate (PET) membranes and one strip of poly tetra fluoroethylene (PTFE) membrane with their edges connected by the dual adhesive tape for harvesting wind energy. Parametric studies are carried out in a wind tunnel to examine its flutter characteristic and improve its power generation. Note that the flag-type TENG can induce flutter with different critical wind speed via adjustments of the bending stiffness (K_B). The flutter frequency can be varied by changing the mass ratio (M^*). The output performance can be influenced by the aspect ratio (L/W). The current study demonstrates the significant advantages of utilizing the flexible electrode for wind energy harvesting especially in natural ambient conditions. The flag-type TENG can be seen to enable self-sustained power generation from arbitrary wind direction without any need of extra mechanisms. More importantly, by conducting humidity test in wind tunnel and rain environment, the flag-type TENG demonstrates stable output performance under high humidity condition.

2. Results and discussion

2.1. Structure and working principle of the flag-type TENG

Fig. 1a illustrates the application scenario of the flag-type TENG. Wind energy is converted to the electricity for powering sensor node, and the weather information can be sent to thermometer screens through wireless communication modules. As shown in Fig. 1b, the flag-type TENG is made of two carbon-coated PET membrane and one strip of PTFE membrane pasted together by araldite. The flag-type TENG works in the freestanding contact mode. The working principle is demonstrated in Fig. 1c. At the original state, the PTFE membrane and carbon electrode are separated. When the wind passes by, the flag starts to flutter, and the PTFE contacts with the carbon electrode. Due to the electronegativity difference between the PTFE and carbon, positive and negative triboelectric charges are generated on the surfaces of the carbon electrode and PTFE membrane respectively. When they are separated, triboelectric electrons flow from the upper carbon electrode to the lower one through the external circuit, and a transient current is generated. When the PTFE membrane comes into contact with the lower carbon electrode, all the positive charges occur on this electrode. Subsequently, the reversed flapping of the PTFE membrane leads to a reversed transfer of electrons through the external circuit. Furthermore, the COMSOL Multiphysics software is employed to calculate the electrostatic field distribution of the TENG. The results are shown in Fig. S1. Apparently, the simulation results are in consistent with the above analysis.

According to the theory of the contact-mode freestanding TENG, the governing equation for TENG can be written as [45]:

$$V = -\frac{1}{C}Q + V_{OC} = -\frac{d_0 + g}{\varepsilon_0 S}Q + \frac{2\sigma x}{\varepsilon_0} \quad (1)$$

Where Q is the total transferred charge, V_{OC} is the open circuit voltage, C, d_0, g, ε_0 and S represent the capacitance of the TENG, the thickness of the membrane, the distance between two electrodes, the dielectric constant in vacuum and the area size of the electrode, respectively; x denotes the displacement between the dielectric membrane and the electrode and σ is the charge density.

2.2. Flutter of the flag-type TENG

Movement-induced excitation (MIE) is a kind of flutter that is considered to be a self-excited vibration resulting from a resonant bending instability of the immersed structure [46,47]. At a certain

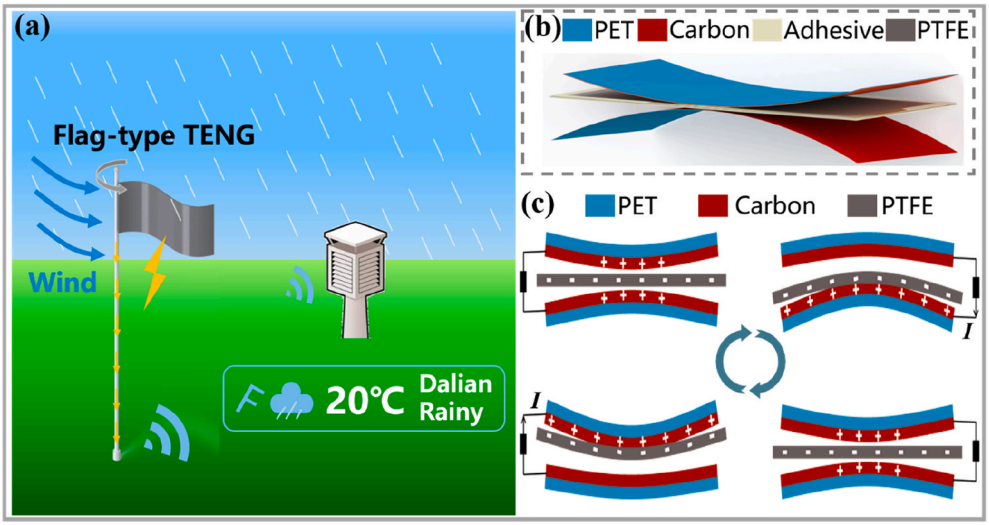

Fig. 1. Application scenario and working mechanism of the flag-type TENG. (a) Application scenario of the flag-type TENG; (b) schematic diagram of the flag-type TENG; (c) working mechanism of the flag-type TENG.

critical flow speed, negative damping of the structure occurs and divergence of structural deformations results. Once the flow speed reaches the critical value, flutter occurs and self-sustain [48]. The flapping of the flag follows the rule of the MIE-flutter. Connell and Yue [49] investigated the flapping stability and response of a thin two-dimensional flag of high extensional rigidity and low bending rigidity. The three relevant non-dimensional parameters governing the flutter are discussed in their work, which are the structure-to-fluid mass ratio (M^*), Reynolds number (Re) and bending stiffness (K_B):

$$M^* = \frac{\rho_s h}{\rho_f L} \tag{2}$$

$$R_e = \frac{\rho_f UL}{\mu} \tag{3}$$

$$K_B = \frac{Eh^3}{12(1-\nu^2)\rho_f U^2 L^3} \tag{4}$$

where μ is viscosity and ν is the Poisson's ratio. ρ_f and ρ_s is the fluid and flag densities respectively; U is the flow speed, h is the thickness of the flag, L is the flag length and E is the Young's modulus.

Argentina and Mahadevan [50] focused on the stability analysis of the flag. The critical speed as well as the flutter frequency of a soft high-density flag immersed in a low-density fluid could be predicted approximately by the following relations:

$$U_c \sim \sqrt{\frac{Eh^3}{\rho_f L^3}} \tag{5}$$

$$f \sim \sqrt{\frac{\rho_f U^2}{\rho_s hL}} \tag{6}$$

here, U_c is the critical flutter speed, f is the flutter frequency, It can be seen in Equations (4) and (5) that the critical speed is related to the bending stiffness (K_B), which also can affect the working wind range of the flag-type TENG. By adjusting the parameters associated with K_B, it is possible to induce flutter for different flag dimensions. In addition, from Equations (2) and (6), the flutter frequency depends on the wind speed and mass ratio (M^*). The contact area is very linked to the aspect ratio (L/W). Therefore, (K_B), (L/W) and (M^*) should be systematically investigated to illustrate the flutter characteristics and electricity generation performance of the flag-type TENG.

Experiments on the parameter relationships for the flag-type TENG are performed in an open-loop low-speed wind tunnel. The schematic of the experimental setup is depicted in Fig. 2a. Fig. 2b shows the flag flutter when the $M^* = 0.43$ and $L/W = 2$ confirming the two dynamic regimes of the flag-type TENG including stable and flutter. The second regimes are also observed for the flag-type TENG with different mass ratios. It also can be observed in Fig. 2b that the amplitude of the flag grows with increasing the wind speed and decreasing the bending

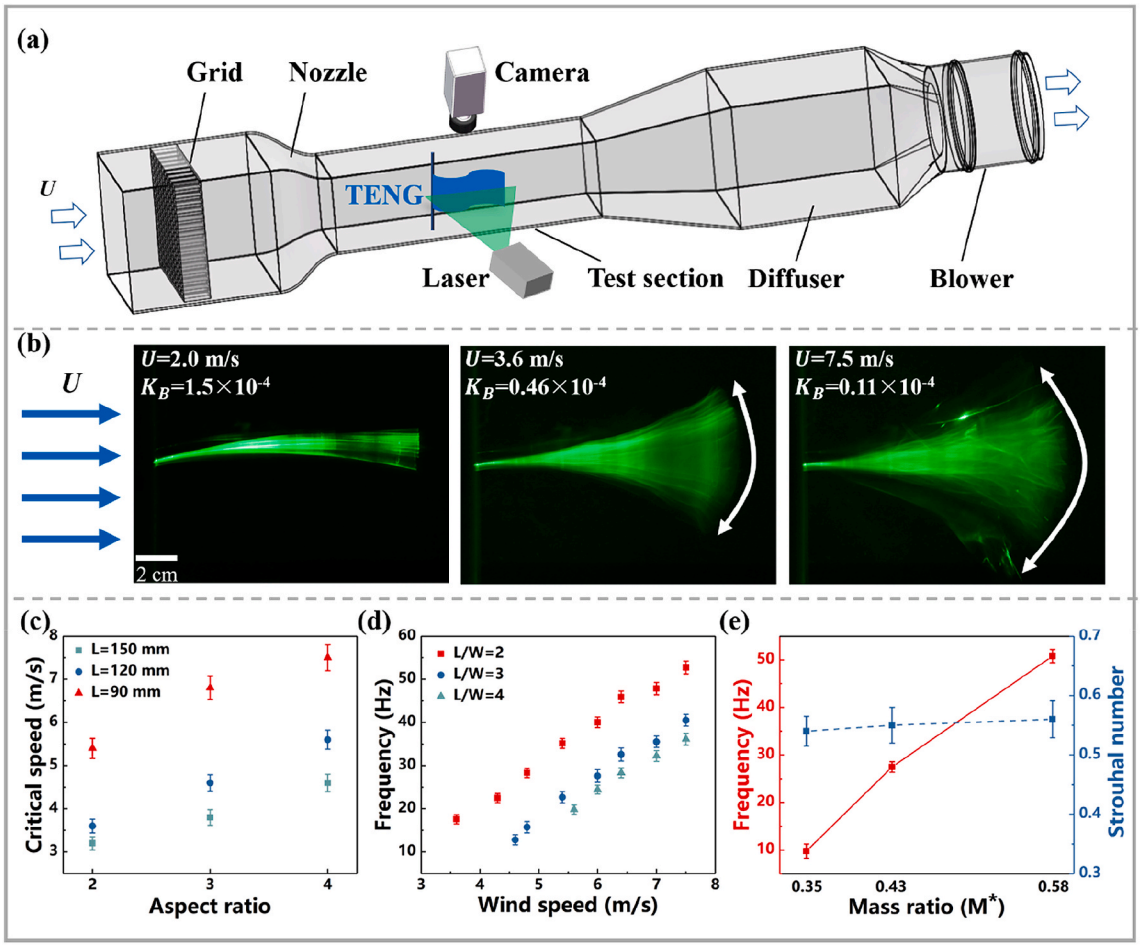

Fig. 2. Schematic of the experimental apparatus and flutter characteristics of the flag-type TENG. (a) Schematic of the experimental apparatus; (b) motion of the flag-type TENG is obtained by superimposing images of different positions at different wind speeds and bending stiffness; (c) effect of the aspect ratio on the critical wind speed with $M^* = 0.43$; (d) dependence of the flutter frequency on wind speed with $M^* = 0.43$; (e) effect of the mass ratio on the frequency and the related Strouhal number.

stiffness. The critical speed of the flag-type TENG for different length and aspect ratio is presented in Fig. 2c. Evidently, the increased flag results in a lower critical speed, which agrees well with Equation (5) or Argentina and Mahadevan [50]. The flutter frequency of the flag is identical to the flag-type TENG output electric signal, which can be obtained by analyzing the signal through Fourier transform. As it can be seen in Fig. 2d, the flutter frequency with different aspect ratios for the case $M^* = 0.43$ is proportional to the wind speed. The similar results are observed for $M^* = 0.35$ and $M^* = 0.58$, see Fig. S2. These observations were made also by Shelley et al. [51]. The flutter frequency of the flag-type TENGs for different mass ratios with $R_e = 40000$ and $K_B = 0.25 \times 10^{-4}$ is presented in Fig. 2e. Apparently, while the flutter frequency is sensitive to the mass ratio, the Strouhal number $S_t = fL/U$ varies little with M^*, in line with the modeling result of Shoele and Mittal [52]. The Strouhal number ranges $S_t \approx 0.5 - 0.6$ for all evaluated cases.

2.3. Electrical output performance of the flag-type TENG

The output performance tests with different materials are conducted in the open loop wind tunnel. A flag-type TENG with the dimension of 150 × 75 mm is first used in the wind tunnel experiment. According to the triboelectric sequence of common materials, benzene type polyimide (Kapton) and PET are selected as the dielectric materials to test the power generation performance of the flag-type TENG. Due to the weaker electronic ability than PTFE and higher Young's modulus than PTFE, the power generation of the flag-type TENG fabricated by PET and Kapton are reduced, and the critical wind speeds are increased as shown in Fig. S3. Significantly, the application of PTFE membrane can improve the electrical output and decrease the critical wind speed of the flag-type TENG effectively. Therefore, the PTFE membrane is adopted for the current work.

The effects of mass and aspect ratios on the energy harvesting performance with controlling wind speed are investigated in the wind tunnel. Wind energy is harvested during flutter regime ($K_B < 0.46 \times 10^{-4}$) for the flag with $M^* = 0.43$ and $L/W = 2$. The flag-type TENG starts to flutter when the bending stiffness decreases below 0.46×10^{-4} as displayed in Supplementary Movie 1. The short circuit current of the flag-type TENG is studied and the results are displayed in Fig. 3a-3c as a function of the wind speed and bending stiffness (K_B). As shown in Fig. 3a-3c, higher current is obtained for lower bending stiffness, mass ratio and aspect ratio. The maximum output current of 0.75 μA is

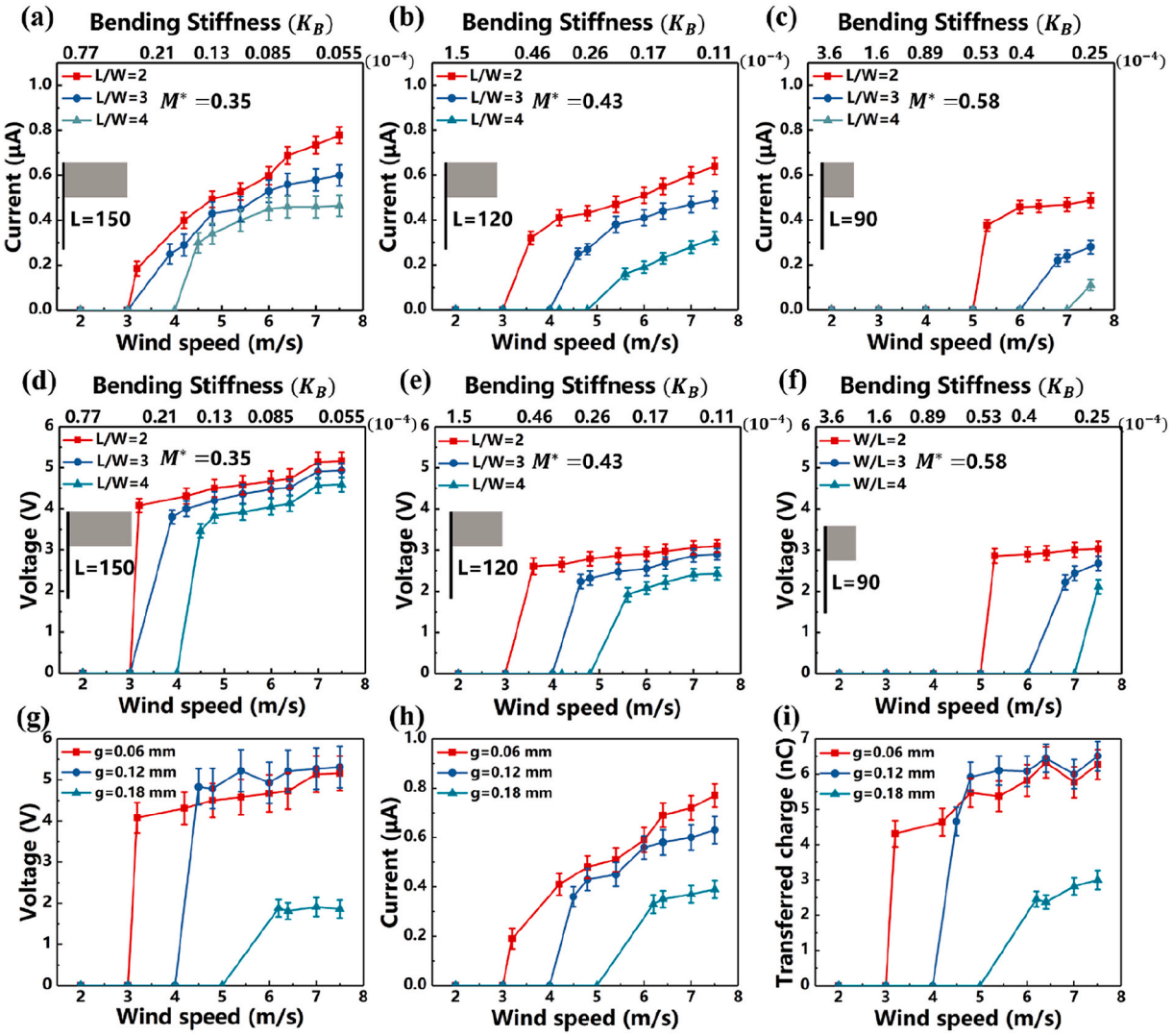

Fig. 3. Output voltage and current *vs.* wind speed and bending stiffness (not to scale) for different aspect ratios (L/W) of the flag-type TENG. (a) short circuit current of the flag with $M^* = 0.35$; (b) short circuit current of the flag with $M^* = 0.43$; (c) short circuit current of the flag with $M^* = 0.58$; (d) open circuit voltage of the flag with $M^* = 0.35$; (e) open circuit voltage of the flag with $M^* = 0.43$; (f) open circuit voltage of the flag with $M^* = 0.58$; (g) open circuit voltage; (h) short circuit current; (i) transferred charge of the flag-type TENG with different distance between two electrodes.

obtained at a wind speed of 7.5 m/s (or $K_B = 0.055 \times 10^{-4}$) when $M^* = 0.35$ and $L/W = 2$ in the open-loop wind tunnel. Higher output current or a significant amount of energy can be observed for higher wind speed as well as a higher flutter frequency. Results from the figure show that the critical speed of the flutter depends on the mass ratio with 3.6 m/s and 5.2 m/s, when $M^* = 0.43$ and $M^* = 0.58$, respectively. An output current of about 0.3 μ*A* is achieved at a low critical wind speed of 3.2 m/s with a flag length of 150 mm as shown in Fig. 3a, which represents a typical ambient wind condition in a city. The similar can be observed in Fig. 3d-3f. The flag-type TENG can be tuned to induce flutter in a low wind speed condition by adjusting the bending stiffness while the mass ratio is constant. The designed flag-type TENG can overcome the limitations of the current wind energy harvesters that have drawbacks in working in ambient wind condition and the working range of wind speed that leads to flutter. It is suggested that the flag-type TENG has potential applications on ambient wind energy harvesting. According to Equation (1), the distance between two electrodes is one of the key parameters that determines its output performance. It can be found in Fig. 3g and 3i that increasing the *(g)* from 0.06 mm to 0.18 mm, the output voltage and transferred charge of the flag-type TENG increase a bit and then decrease. This may be explained by the fact that although *(g)* increases, the increase in bending stiffness results in the decreasing of the contact area of the PTFE and flexible electrode. Increasing the thickness of the flag results in the lower frequency according to Equation (6), therefore the current decreases as shown in Fig. 3h. In addition, the critical wind speed increases dramatically with the growing of *(g)*. It is not appropriate to enhance the output performance by increasing the parameter *(g)*.

Supplementary video related to this article can be found at https://doi.org/10.1016/j.nanoen.2020.105279

The output performance of TENGs can be substantially influenced by the surrounding environment, especially the relative humidity (RH). The adsorption of the water vapor on the surface of the PTFE surface can reduce charges generated by the contact electrification or can discharge the surface [53]. Another benefit of adopting the flag-type TENG for wind energy harvesting is the humidity resisting characteristic that ensures the flag-type TENG to work properly under high humidity conditions. In order to avoid contact between PTFE and water vapor in the air. The electrode and PTFE membrane are enclosed in the PET. The triboelectric layers are isolated from the air, power generation performance of the flag-type TENG cannot be affected by the relative humidity of the air. The humidity tests are conducted as shown in Fig. 4a. The experimental results show that no obvious difference in the output voltage, current and transferred charge are observed with different relative humidity conditions as shown in Fig. 4b-4d. Guo et al. [43] invented an ATNG to detect humidity and airflow rate. With RH increasing from 20% to 100% the output voltage dropped from 36 V to 18 V. Zhao et al. [40] designed a WTENG flag for wind energy harvesting. At RH 96% condition, the output current sharply decreased to 8 μ*A* from 22 μ*A*. Phan et al. [44] invented a TENG flowmeter. The output current decreased

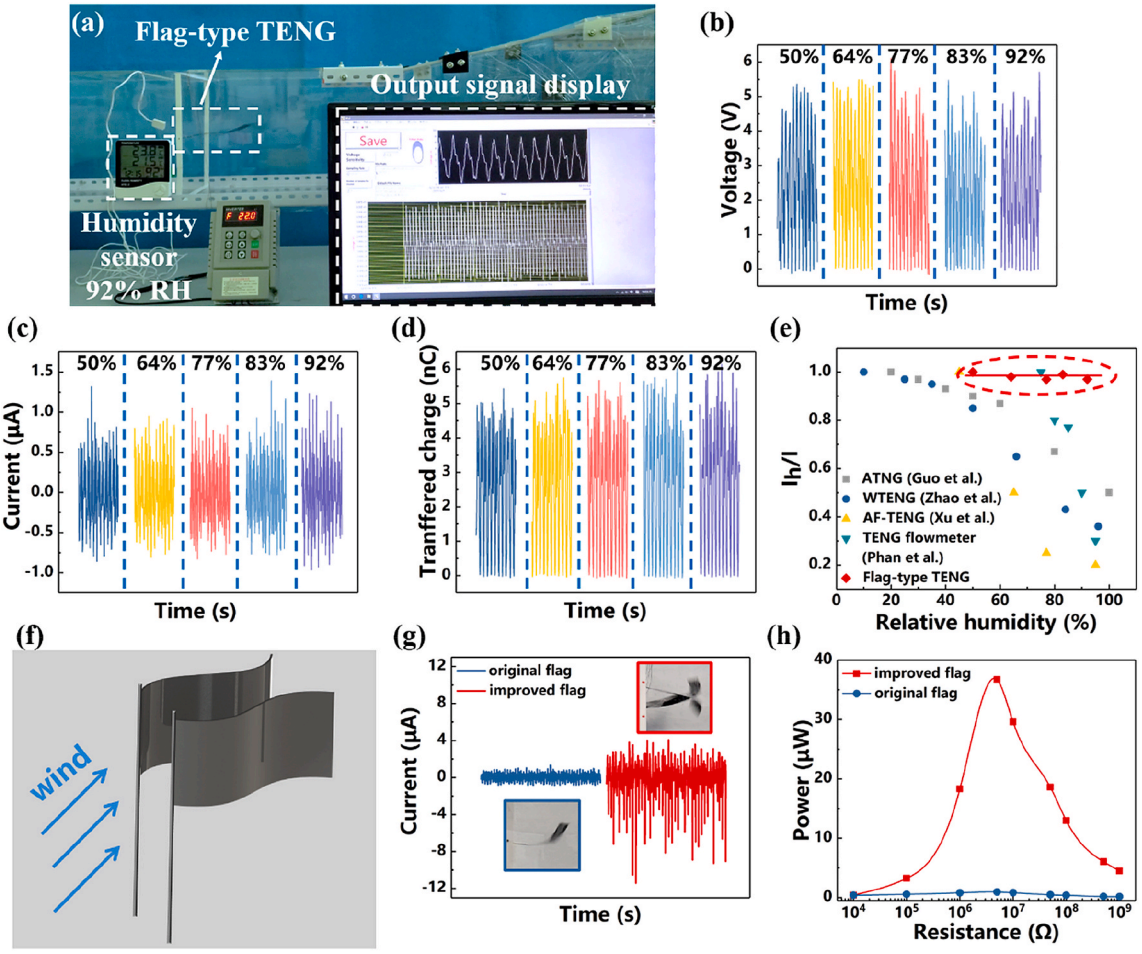

Fig. 4. Effect of the relative humidity on the power generation performance of the flag-type TENG. (a) schematic of the experimental apparatus; (b) open circuit voltage; (c) short circuit current; (d) transferred charge of the flag-type TENG; (e) the present performance versus those previously of ATNG [43], WTENG flag [40], TENG flowmeter [44] and AF-TENG [29]; (d) photograph of the flag-type TENG; (f) schematic of the 2 flag-type TENGs fixed with a certain gap distance for improving its performance; (g) output current comparison of the improved flag with the original flag; (h) output power comparison of the improved flag with the original flag.

from 0.8 μ*A* to 0.2 μ*A* by increasing the humidity from 75% to 95%. An aeroelastic flutter TENG was proposed by Xu et al. [29] to measure the wind speed. They found that the current and voltage output can decrease by nearly 90% by changing the humidity from 45% to 95%. Fig. 4e demonstrates that by normalizing the output current in different RH, the flag-type TENG keeps a stable output current; here I_h is the output current at different RH, I is the maximum output current. Supplementary Movie 2 shows that the wind energy can be harvested effectively even on rainy condition. The output current keeps almost constant throughout the process as shown in Fig. S4. In addition, a comparison experiment is conducted to verify the non-dependence of output performance on humidity as illustrated in Supplementary Movie 3. The output performance is tested at 77% and 92% RH, and there is no significant difference in performance.

Supplementary video related to this article can be found at https://doi.org/10.1016/j.nanoen.2020.105279

In order to further improve the power generation performance of the flag-type TENG, 2 flag-type TENGs are fixed with a certain gap distance as shown in Fig. 4f. When the wind flows, the two flags flutter and come into contact with each other due to the wind speed variation and pressure difference between the internal and external flow areas as depicted in Supplementary Movie 4. According to the results from Sun et al. [54], the optimal gap distance is about 35 mm. In this way, the contact area between the PTFE and the electrode of the flag is increased. The output voltage and current of a flag-type TENG increase to 20.8 V and 6.8 μ*A* from 5 V, 0.75 μ*A*, as shown in Fig. S5 and Fig. 4g. Under the matched loading resistance of 5 MΩ, the peak output power of the flag-type TENG increases to 36.72 μ*W* with the corresponding volume power density of 0.0408 mW/cm^3, compared with the original flag, the power is increased by 40 times (Fig. 4h). The voltage of a 50 μ*F* capacitor can be charged to 3 V in 150 s as shown in Fig. S6. The device output current is consistent over 300 s in 3 days at a relative humidity of 92% as depicted in Fig. S7, implying that the device is durable. As shown in Supporting Table 1, Some previous wind energy harvesting TENGs are summarized. The performance of the flag-type TENG is not inferior in low wind speed conditions.

Supplementary video related to this article can be found at https://doi.org/10.1016/j.nanoen.2020.105279

The dielectric membrane is confined in a case or frame for most of previously reported wind energy harvesting TENGs. However, this configuration limits the harvesting wind energy from arbitrary direction, considering that the wind in nature is often astatic. The flag-type TENG can tune itself to any wind directions without extra mechanisms. An antifriction bearing is installed to ensure it able to rotate 360° as shown in Fig. S8. As exhibited in Fig. 5a-5c, the flag-type TENG with a dimension of 150 × 75 mm shows a constant output performance when the wind direction changes in any direction, indicating that the wind energy can be effectively harvested from arbitrary directions. A circuit is designed for wind energy harvesting from arbitrary directions as it is able to power LED, which is presented in Fig. 5d. The flag-type TENG drives the switch which is connected with the bottom of the flagpole, the LED of the corresponding direction is light when the wind moves the flag to the direction as shown in Fig. 5e and Supplementary Movie 5. Therefore, it can also be used for indicating the real-time wind direction.

Supplementary video related to this article can be found at https://doi.org/10.1016/j.nanoen.2020.105279

2.4. Demonstrations of the flag-type TENG

The demonstration experiments are conducted to illustrate the application of the flag-type TENG. The electrical output performance can be improved by connecting manifold flag-type TENGs in parallel. The structure diagram of the integrated devices composed of 2 flag-type TENGs and the circuit are presented in Fig. 6a. As seen in Fig. 6b, a thermometer can be powered by 2 flag-type TENGs. The video for powering a thermometer is shown in Supplementary Movie 6. Fig. 6c demonstrates that the thermometer is successfully lit up after 100 s charging of the 100 μF capacitor. Meanwhile, the flag-type TENG can be used as a self-powered wind speed sensor. Since the frequency of the flag-type TENG output electric signal equals the flutter frequency, the flag-type TENG provides a feasible way to measure the wind speed. Fig. 6d shows the block diagram of flag-type TENG for wind speed sensing. The wind speed U is obtained using the relationship between the frequency of open circuit voltage (V_{oc}) and wind speed, *i.e.* $U = af$,

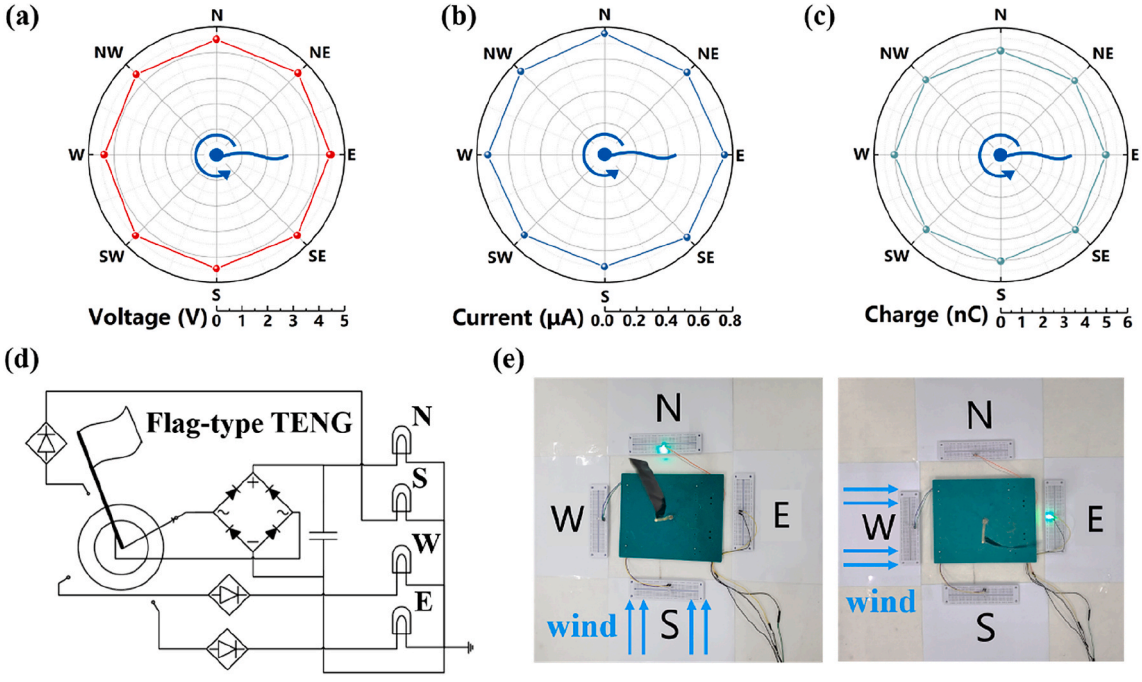

Fig. 5. Dependence of the power generation performance of the flag-type TENG on the wind direction; (a) open circuit voltage, (b) short circuit current, and (c) transferred charge of the flag-type TENG; (d) circuit design; (e) photograph of the flag-type TENG for harvesting wind energy form different directions.

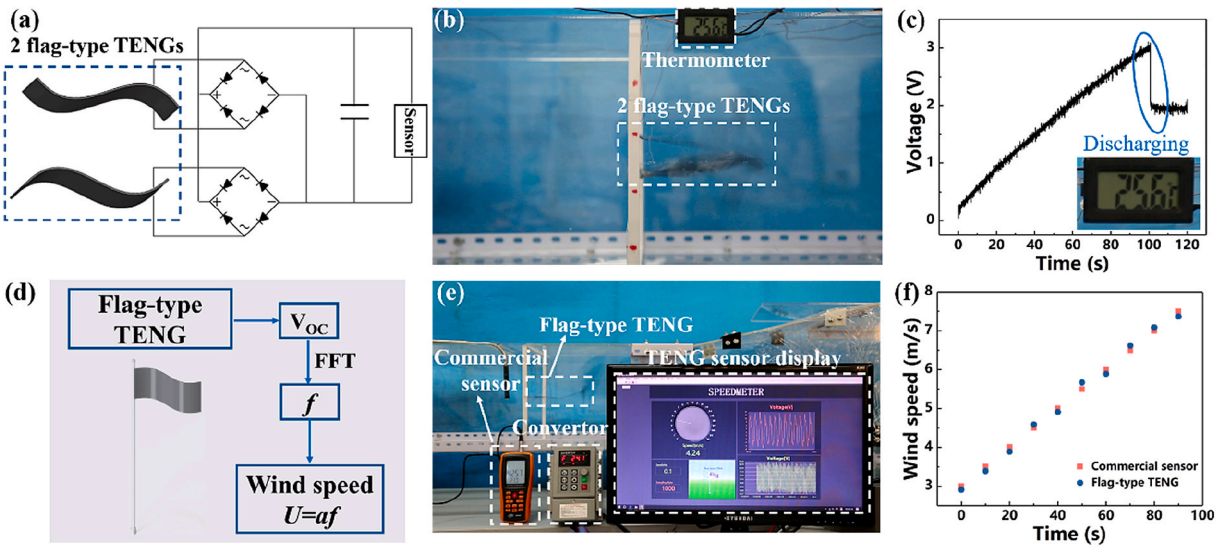

Fig. 6. Demonstration of the flag-type TENG. (a) schematic diagram of 2 flag-type TENGs and working circuit to power light or sensor; (b) the photograph a thermometer powered by 2 flag-type TENGs; (c) powering a thermometer with 2 flag-type TENGs; (d) schematic diagram of flag-type TENG for wind speed sensing; (e) photograph of the real-time wind speed measurement using the flag-type TENG and a commercial sensor; (f) comparison of the flag-type TENG and commercial wind speed sensor.

where a is a constant coefficient, here with $a = 0.31$. The wind speed signal is sent to a computer as presented in Fig. 6e and Supplementary Movie 7. The real-time wind speed obtained by the flag-type TENG and a commercial anemometer are compared and they agree well as depicted in Fig. 6f. Therefore, the flag-type TENG can be used as a self-powered wind speed sensor.

Supplementary video related to this article can be found at https://doi.org/10.1016/j.nanoen.2020.105279

3. Conclusion

This work has successfully developed a humidity resisting and wind direction adapting flag-type TENG that can harvest wind energy and additionally measure wind speed. In particular, this flag-type TENG can be induced to flutter by a wind with the velocity ≥3.2 m/s via adjusting the flag bending stiffness ($K_B = 0.21 \times 10^{-4}$). By conducting performance test experiments in a wind tunnel, a structure-optimized flag-type TENG with the aspect ratio ($L/W = 2$) and dimension 150 × 75 mm has been developed. The power generation of the flag-type TENG was found to increase with decreasing bending stiffness and mass ratio. Significantly, the flag-type TENG shows a superior output performance as the wind direction varies. The flag-type TENG is able to harvest wind energy from arbitrary directions. In order to further improve the power generation performance of the flag-type TENG, two flag-type TENGs are fixed with a certain gap distance. They can contact with each other due to the wind speed variation and pressure difference between the internal and external flow areas. The power density is increased by 40 times compared with the only one flag-type TENG. A maximum current of 6.8 μA and a peak output power of 36.72 μW were achieved under the matched loading resistance of 5 MΩ at the wind speed of 7.5 m/s. Meanwhile, the flag-type TENG can be used as a sensor to measure the wind speed and indicate wind direction. More importantly, the flag-type TENG can be utilized in a humidity condition to effectively harvest wind energy. This allows it to work in many natural conditions. Therefore, the as-fabricated flag-type TENG has shown great potential applications in wind energy harvesting and self-powered wind speed & direction sensing at humidity conditions.

4. Experimental section

4.1. Manufacture of the flag-type TENG

The fabrication of the flag-type TENG is shown in Fig. 1a. The PTFE, PET membranes and dual adhesive tape are, respectively, 30 μm, 25 μm and 30 μm in thickness. The width of the 3M200C dual adhesive tape are 2 mm. A conductive carbon ink electrode with a micrometer thickness was attached to the back side of the PET to serve as the flexible electrode. The flag-type TENG is composed of two flexible electrodes and one strip of PTFE membrane with their edges sealed up by dual adhesive tapes with its thickness of 30 μm. Thus, the gap distance between the flexible electrode and PTFE can be adjusted by using multiple layers of the dual adhesive tape. The flag-type TENG and the flagpole are connected together by the sticky tape. The integrated device is set in a antifriction bearing to ensure it able to rotate 360° as shown in Fig. S8. When wind flows along the flag-type TENG, the flag can flutter periodically and tune itself with wind direction, thus producing alternating voltage and current signals.

4.2. Electrical output measurement

The experiments for the flag-type TENG are performed in a wind tunnel with a dimension of 0.25 m (width) × 0.25 m (height) × 1.0 m (length). The wind speed varies from 2.0 m/s to 7.5 m/s. The blower is installed at the right end of the wind tunnel. An inverter is used to control the rotating speed of the blower which can control the wind speed. A humidifier is placed at the entrance of the wind tunnel to control the relative humidity as shown in Fig. S9. To measure the electrical output of the flag-type TENG, a programmable electrometer (Keithley Model 6514) is used.

CRediT author contribution statement

Yan Wang: Conceptualization, Methodology, Writing - original draft. **En Yang:** Formal analysis, Data curation. **Tianyu Chen:** Validation. **Jianye Wang:** Demonstration experiments performing. **Zhiyuan Hu:** Software. **Jianchun Mi:** Writing - review & editing. **Xinxiang Pan:** Funding acquisition. **Minyi Xu:** Supervision, Writing - review & editing.

Declaration of competing interest

The authors declare that they have no known competing financial interests or personal relationships that could have appeared to influence the work reported in this paper.

Acknowledgments

Y. Wang and E. Yang contribute equally to this work. The authors are grateful for the joint support from the National Natural Science Foundation of China (Grant Nos. 51879022, 51979045, 51906029), the Fundamental Research Funds for the Central Universities, China (Grant No. 3132019330), and Projects for Dalian Youth Star of Science and Technology (Grant No. 2018RQ12).

Appendix A. Supplementary data

Supplementary data to this article can be found online at https://doi.org/10.1016/j.nanoen.2020.105279.

References

[1] W.V. Schalkwijk, B. Scrosati, Advances in Lithium-Ion Batteries, Springer, Boston, US, 2002.
[2] B. Scrosati, Chem. Rec. 5 (2005) 286–297.
[3] R. Datta, V.T. Ranganathan, IEEE Trans. Power Electron. 16 (2002) 390–399.
[4] M. Armandei, A.C. Fernandes, A.B. Rostami, Exp. Tech. 40 (2015) 833–839.
[5] D. Ramasur, G.P. Hancke, in: Instrumentation and Measurement Technology Conference (I2MTC), 2012, IEEE International, 2012, pp. 2623–2627.
[6] S. Priya, C.T. Chen, D. Fye, J. Zahnd, Jpn. J. Appl. Phys. 44 (2005) 1–7.
[7] D. Vu, V. Nguyen, T. Dinh, V. Huy, Energy Sustain. Dev. 33 (2016) 75–83.
[8] J. Hu, X. Pu, H. Yang, Q. Zeng, Q. Tang, D. Zhang, C. Hu, Y. Xi, Nano Res. 12 (2019) 3018–3023.
[9] S. Roundy, P.K. Wright, Smart Mater. Struct. 13 (2004) 1131–1142.
[10] J. Wang, L. Geng, L. Ding, H. Zhu, D. Yurchenko, Appl. Energy 267 (2020) 114902.
[11] J.M. McCarthy, A. Deivasigamani, S.J. John, S. Watkins, F. Coman, P. Petersen, Exp. Therm. Fluid Sci. 51 (2013) 279–290.
[12] Y. Liu, R. Bao, J. Tao, J. Li, M. Dong, C. Pan, Sci. Bull. 65 (2020) 70–88.
[13] J. Sun, A. Yang, C. Zhao, F. Liua, Z. Li, Sci. Bull. 64 (2019) 1336–1347.
[14] F. Wu, C. Li, Y. Yin, R. Cao, H. Li, X. Zhang, S. Zhao, J. Wang, B. Wang, Y. Xing, X. Du, Adv. Mater. Technol. 4 (2018) 1800216.
[15] C. Lu, J. Chen, T. Jiang, G. Gu, W. Tang, Adv. Mater. Technol. 3 (2018) 1800021.
[16] S. Orrego, K. Shoele, A. Ruas, K. Doran, B. Caggiano, R. Mittal, S.H. Kang, Appl. Energy 194 (2017) 212–222.
[17] J. McCarthy, School of Aerospace, Mechanical and Manufacturing Engineering, RMIT University, 2015.
[18] T. Ackermann, L. Soder, Renew. Sustain. Energy Rev. 4 (2000) 315–374.
[19] A.I. Aquino, J.K. Calautit, B.R. Hughes, Energy Procedia 142 (2017) 321–327.
[20] M. Xu, P. Wang, Y. Wang, S.L. Zhang, A.C. Wang, C. Zhang, Z. Wang, X. Pan, Z. L. Wang, Adv. Energy Mater. 8 (2018) 1702432.
[21] X. Xiao, X. Zhang, S. Wang, H. Ouyang, P. Chen, L. Song, H. Yuan, Y. Ji, P. Wang, Z. Li, M. Xu, Z.L. Wang, Adv. Energy Mater. 9 (2019) 1902460.
[22] M. Xu, S. Wang, S.L. Zhang, W. Ding, K.T. Phan, C. Wang, Z. Li, X. Pan, Z.L. Wang, Nano Energy 57 (2019) 574–580.
[23] X. Zhang, M. Yu, Z. Ma, H. Ouyang, Y. Zou, S.L. Zhang, H. Niu, X. Pan, M. Xu, Z. Li, Z.L. Wang, Adv. Funct. Mater. 29 (2019) 1900327.
[24] F.-R. Fan, Z.-Q. Tian, Z. Lin Wang, Nano Energy 1 (2012) 328–334.
[25] H. Zhao, X. Xiao, P. Xu, T. Zhao, L. Song, X. Pan, J. Mi, M. Xu, Z.L. Wang, Adv. Energy Mater. 9 (2019) 1902824.
[26] M. Ma, Z. Zhang, Q. Liao, G. Zhang, F. Gao, X. Zhao, Q. Zhang, X. Xun, Z. Zhang, Y. Zhang, Nano Energy 39 (2017) 524–531.
[27] Z. Quan, B. Chang, J. Tao, Z.L. Wang, Adv. Energy Mater. 6 (2016) 1501799.
[28] H. Phan, D. Shin, H. Sang, Y. Tae, P. Han, G. Kim, H. Kim, K. Kim, Y. Hwang, S. Hong, Nano Energy 33 (2017) 476–484.
[29] M. Xu, Y. Wang, S.L. Zhang, W. Ding, J. Cheng, X. He, P. Zhang, Z. Wang, X. Pan, Z. L. Wang, Extrem. Mech. Lett. 15 (2017) 122–129.
[30] Y. Bian, T. Jiang, T. Xiao, W. Gong, X. Cao, Z. Wang, Z.L. Wang, Adv. Mater. Technol. 3 (2018) 1700317.
[31] Y. Wang, J. Wang, X. Xiao, S. Wang, T.K. Phan, J. Dong, J. Mi, X. Pan, H. Wang, M. Xu, Nano Energy 73 (2020) 104736.
[32] D. Liu, B. Chen, J. An, C. Li, G. Liu, J. Shao, W. Tang, C. Zhang, Z.L. Wang, Nano Energy 73 (2020) 104819.
[33] Y. Yang, G. Zhu, H. Zhang, J. Chen, X. Zhong, Z.-H. Lin, Y. Su, P. Bai, X. Wen, Z. L. Wang, ACS Nano 7 (2013) 9461–9468.
[34] Y. Su, G. Xie, X. Tao, H. Zhang, Z. Ye, Q. Jing, H. Tai, X. Du, Y. Jiang, J. Phys. D Appl. Phys. 49 (2016) 215601.
[35] S. Wang, X. Mu, Y. Yang, C. Sun, A.Y. Gu, Z.L. Wang, Adv. Mater. 27 (2015) 240–248.
[36] H. Zheng, Y. Zi, X. He, H. Guo, Y.C. Lai, J. Wang, S.L. Zhang, C. Wu, G. Cheng, Z. L. Wang, ACS Appl. Mater. Interfaces 10 (2018) 14708–14715.
[37] J. Bae, J. Lee, S. Kim, J. Ha, B.-S. Lee, Y. Park, C. Choong, J.-B. Kim, Z.L. Wang, H.-Y. Kim, J.-J. Park, U.-I. Chung, Nat. Commun. 5 (2014) 4929.
[38] S. Wang, X. Mu, X. Wang, A.Y. Gu, Z.L. Wang, Y. Yang, ACS Nano 9 (2015) 9554–9563.
[39] M. Perez, S. Boisseau, P. Gasnier, J. Willemin, J.L. Reboud, Smart Mater. Struct. 24 (2015), 035004.
[40] Z. Zhao, X. Pu, C. Du, L. Li, C. Jiang, W. Hu, Z.L. Wang, ACS Nano 10 (2016) 1780–1787.
[41] V. Nguyen, R. Yang, Nano Energy 2 (2013) 604–608.
[42] T.-H. Chang, Y.-W. Peng, C.-H. Chen, T.-W. Chang, J.-M. Wu, J.-C. Hwang, J.-Y. Gan, Z.-H. Lin, Nano Energy 21 (2016) 238–246.
[43] H. Guo, J. Chen, L. Tian, Q. Leng, Y. Xi, C. Hu, ACS Appl. Mater. Interfaces 6 (2014) 17184–17189.
[44] T.K. Phan, S. Wang, Y. Wang, H. Wang, X. Xiao, X. Pan, M. Xu, J. Mi, Sensors 20 (2020) 729.
[45] S. Niu, Y. Liu, X. Chen, S. Wang, Y.S. Zhou, L. Lin, Y. Xie, Z.L. Wang, Nano Energy 12 (2015) 760–774.
[46] E. Naudascher, D. Rockwell, J. Hydraul. Res. 18 (1980) 59–82.
[47] A. Khalak, C.H.K. Williamson, J. Fluid Struct. 13 (1999) 813–851.
[48] A. Eaton Lombard, California Institute of Technology, 1939.
[49] B.S.H. Connell, D.K.P. Yue, J. Fluid Mech. 581 (2007) 33–67.
[50] M. Argentina, L. Mahadevan, Proc. Natl. Acad. Sci. U.S.A. 102 (2004) 1829–1834.
[51] M. Shelley, N. Vandenberghe, J. Zhang, Phys. Rev. Lett. 94 (2005), 094302.
[52] S. Kourosh, M. Rajat, J. Fluid Mech. 790 (2016) 582–606.
[53] L.S. McCarty, G.M. Whitesides, Angew. Chem. Int. Ed. 47 (2008) 2188–2207.
[54] W. Sun, Z. Ding, Z. Qin, F. Chu, Q. Han, Nano Energy 70 (2020) 104526.

Yan Wang is currently pursuing his doctor degree in Dalian Maritime University, China. His current research interests include flow induced vibration, blue energy, self-powered systems and triboelectric nanogenerators.

En Yang received his master degree in Dalian Maritime University, China. His research focuses on triboelectric nanogenerators and flutter energy harvesting.

Tianyu Chen is currently pursuing the master degree in Dalian Maritime University, China. His current research interests are triboelectric nanogenerators and their application to ocean wave energy harvesting.

Jianye Wang is currently studying for his master degree at Dalian Maritime University. His current research interests include wind energy, wave energy, Triboelectric Nanogenerators and self-powered systems.

Zhiyuan Hu is currently pursuing his master degree in Dalian Maritime University, China. His current research interests are triboelectric nanogenerators and power management module.

Prof. Jianchun Mi received his Ph.D. degrees from Newcastle University in 1995. He was a national researcher and director researcher of Adelaide University in Australia from 1995 to 2006. He joined Peking University in 2006, and now he is a full professor in the College of Engineering. His research interests include turbulence, combustion and renewable energy.

Xinxiang Pan received his B.E and Ph.D. degrees from Marine Engineering College, Dalian Maritime University, China, in 1987 and 1999. He now is President of Guangdong Ocean University. His research interests include smart and green ship, ocean engineering, energy saving and emission reduction, ship safety and pollution control, microfluidic chip, nano energy and self-powered systems.

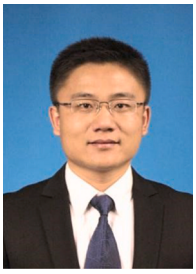

Dr. Minyi Xu received his Ph.D. degree from Peking University in 2012. During 2016–2017, he joined Professor Zhong Lin Wang' group at Georgia Institute of Technology. Now he is a Professor in the Marine Engineering College, Dalian Maritime University. His current research is mainly focused on the areas of blue energy, self-powered systems, triboelectric nanogenerators and its practical applications in smart ship and ocean.